Electronic Supplementary Information for Soft Matter manuscript: Catalytic Janus Swimming Devices with Well Defined Spin by Glancing Angle Metal Evaporation

Richard Archer, Andrew I Campbell, and Stephen J Ebbens*

S1 Video Files of Spinning Spheres

Video 1: Microswimmer produced from colloidal crystal without tilt (high angle) with a velocity to angular velocity ratio (R value) of 0.05.
Video 2: Microswimmer produced from colloidal crystal at slightly tilted angle showing low induced angular velocity with an R value of 0.23.
Video 3: Microswimmer produced from colloidal crystal at medium tilted angle showing medium induced angular velocity with an R value of 0.39.
Video 4: Microswimmer produced from colloidal crystal at highly tilted angle showing high induced angular velocity with an R value of 0.78.

S2 Trajectories of Sparsely Spread Spheres

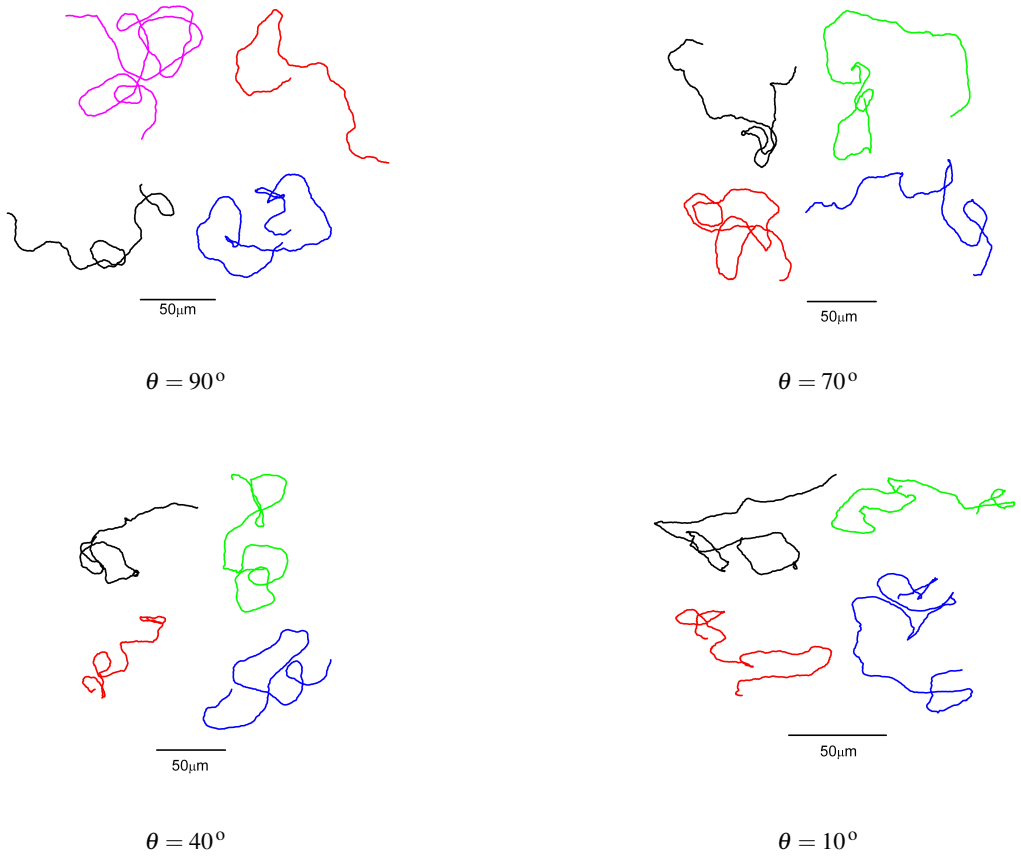

Fig. S1 Representative (x, y) plot trajectories (30 s) for $1.9\,\mu$m diameter Janus colloids re-dispersed into 10 % H_2O_2 solutions after platinum evaporation onto sparsely spread, spun-coat colloids, at a range of glancing angles.

Dept. Chem. and Bio. Eng., The University of Sheffield, Mappin Street, Sheffield, S1 3JD, UK. Fax: +44 (0)114 2227501; Tel: +44 (0)114 2227589; E-mail: s.ebbens@sheffield.ac.uk

S3 Modelling the Shadowed Evaporation Process

Evaporation of a metal, under high vacuum, onto a monolayer of touching colloidal spheres in a hexagonal arrangement produces a catalytic cap geometry that is dependent upon the glancing angle of the metal vapour θ and the orientation of the crystal domain α. Shadowing by spheres blocks the metal vapour from reaching their neighbours changing the shape of the catalytic cap formed and resulting in the angle dependent angular velocity of our swimming Janus spheres. To quantify the change in cap shape and area with α and θ we modelled the cap geometry by following the model described by Pawar *et al*[1]. In previous experiments[2] we have shown that weight of the full hemispherical cap is consistent with an elliptical layer of the catalytic material due to the directional nature of the evaporation process under high vacuum. The cap is thickest at the sphere pole, tapering to a thickness of 0 nm at the equatorial plane of the sphere. The rate of the reaction at the catalytic cap (and velocity of our swimmers) is dependent upon the thickness of the platinum layer, so we also model the thickness of the catalytic cap. Here we describe in some detail the Matlab algorithms used to model the evaporation process.

S3.1 Step 1: Hexagonal Arrangement of Spheres

We generated a 6 x 6 grid of (x_c, y_c, z_c) centre coordinates of touching spheres of radius $r = 1.0$ and crystal orientation $\alpha = 0^o$ on a flat plane ($z = r$, Fig. S2a, b). Where we required $\alpha > 0^o$ we rotated the crystal domain by α degrees to produce the desired orientation (see Fig. S2c).

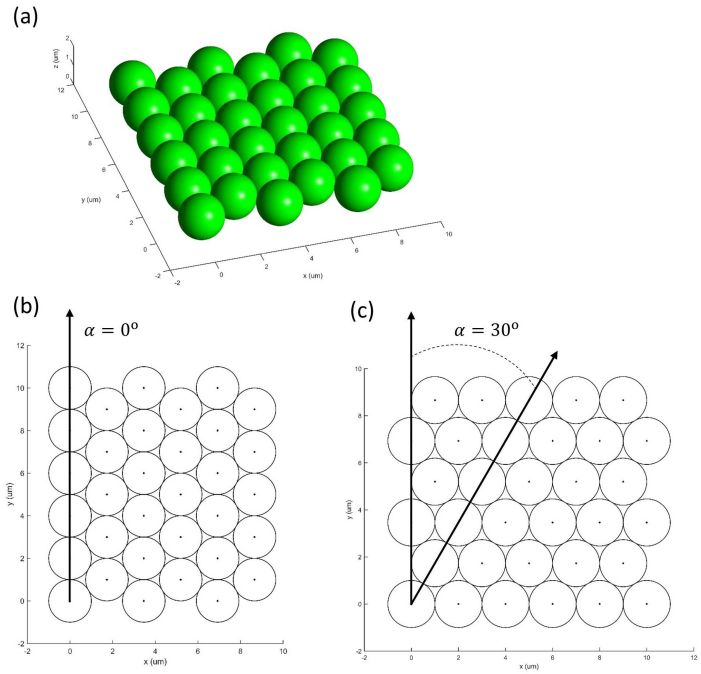

Fig. S2 (a) A 3D hexagonal array of touching spheres on a flat plane. (b) A crystalline array of spheres with an orientation of $\alpha = 0^o$. (c) The same as (b) after rotating to give $\alpha = 30^o$.

S3.2 Step 2: Catalytic Cap Boundary

For widely separated particles on a surface the evaporation of a metal, under high vacuum, results in a uniform coating over one hemisphere of the particles, where the boundary of the coating is positioned at the equatorial plane of the spheres. To simplify the modelling process, we divide our collection of touching spheres into a series of vertical planes along the y-axis and parallel to the (x,z) plane at a separation distance of $0.0005r$. This series of planes divide the spheres into a series of cross-sectional circles, where a circles radius r_c is dependent on the distance of the plane from the sphere centre. The metal vapour being evaporated onto a hexagonal array of spheres is modelled as a set of ray lines, pointing from high to low x and incident upon the cross-sectional circles with glancing angle θ (Fig. S3), with a spacing of $0.0005r$ along the x-axis. Ray lines cannot pass through a circle. The equatorial plane marking the coating boundary on widely separated particles is defined as the point at which the ray lines are tangent to the cross-sectional circle surface. Ray lines

are not blocked by a circle they are tangent to. The right (x_r, z_r) and left (x_l, z_l) tangent boundary points are given by

$$x_r = r_c \cos(\theta - 90) + x_c \tag{S1}$$

$$z_r = r_c \sin(\theta - 90) + z_c \tag{S2}$$

$$x_l = r_c \cos(\theta + 90) + x_c \tag{S3}$$

$$z_l = r_c \sin(\theta + 90) + z_c, \tag{S4}$$

where (x_c, z_c) are the circle centre coordinates.

Our spheres are not widely separated but touching. Working from high to low x (right to left) only the leading circles on the right of the modelled array have both right and left tangent boundaries, forming a uniform coating. Depending on α and θ the right hand tangent lines for the remaining circles may be blocked by their neighbours to the right; i.e. they may be in shadow. Where a tangent line is blocked by a neighbouring circle, the left hand tangent line of the circle to the right continues on to form the right hand boundary point of its neighbour to the left (see Fig. S3). This boundary point marks the shadowed edge of the coating and is located at the intercept between the evaporated metal ray line

$$z_r = \tan\theta \, x - \tan\theta \, x_0, \tag{S5}$$

which intercepts the surface on which the spheres are arranged at x_0, and the circle

$$r_c^2 = (x - x_c)^2 + (z - z_c)^2. \tag{S6}$$

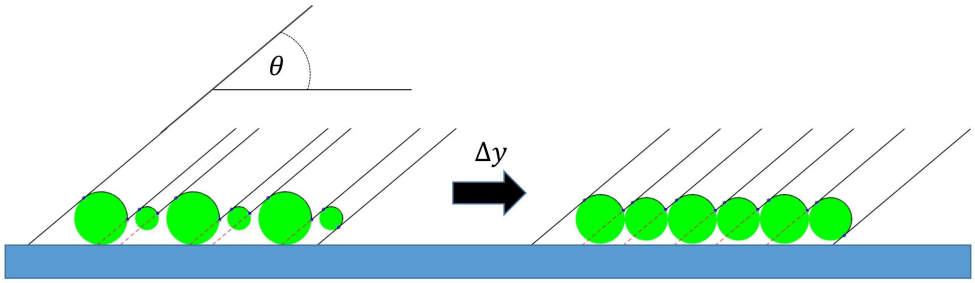

Fig. S3 Taking a series of vertical planes along the y-axis divides the array of spheres in to cross-sectional circles. The metal vapour ray lines, with glancing angle θ, tangent to the circles define the boundary points of the catalytic cap (blue cirlces). Note that circles can shadow their neighbours to the left.

Equation S6 can be expanded to give

$$x^2 - 2xx_c + x_c^2 + z^2 - 2zz_c + z_c^2 - r_c^2 = 0. \tag{S7}$$

Equation S7 can then be solved for x by using $z = z_r$

$$(1 + m^2)x^2 + 2(-x_c - m^2 x_0 - m z_c)x + x_c^2 + m^2 x_0^2 + 2m x_0 z_c + z_c^2 - r_c^2 = 0, \tag{S8}$$

$(m = \tan\theta)$ and using the quadratic formula to find x

$$x = \frac{-b \pm \sqrt{b^2 - 4ac}}{2a}, \tag{S9a}$$

$$a = 1 + m^2, \tag{S9b}$$

$$b = 2(-x_c - m^2 x_0 - m z_c), \tag{S9c}$$

$$c = x_c^2 + m^2 x_0^2 + 2m x_0 z_c + z_c^2 - r_c^2. \tag{S9d}$$

Ray lines cannot pass through a circle so the highest value of x is accepted. With x known the z-coordinate can be found. Boundary coordinates are found for each circle in each vertical plane along the y-axis, generating a list of (x, y, z) catalytic

cap boundary coordinates for each sphere in the array (see Fig. S4).

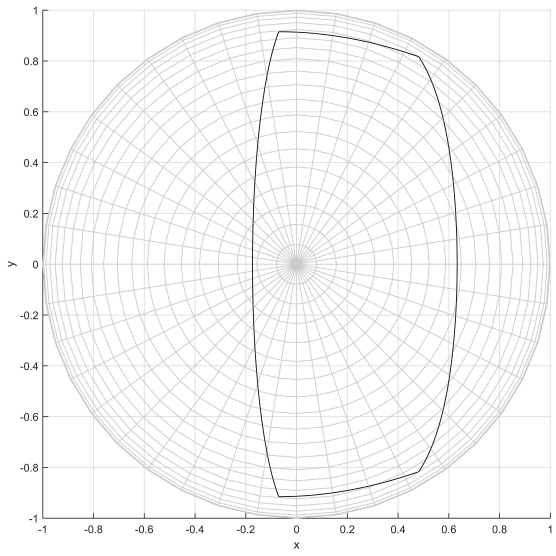

Fig. S4 The boundary of the catalytic cap for $\alpha = 30^{\circ}$ and $\theta = 10^{\circ}$.

S3.3 Step 3: Fill Points

For spheres near the centre of the array the shape of the catalytic cap is the same. We selected a single sphere near the centre of the array and calculated the position of catalytic cap points between the boundary points. The position of the catalytic cap points were calculated using equations (S5) to (S8) and equation S9, with a spacing of $0.0005r$ along both the x and y-axes. We modelled the thickness of the catalytic cap by calculating the cosine of the angle between the incident ray line and the surface normal vector of the sphere and multiplying by the maximum thickness of the evaporated layer (10 nm). The cosine of the angle between the vectors is calculated by dividing the dot product of the vectors by the product of their magnitudes.

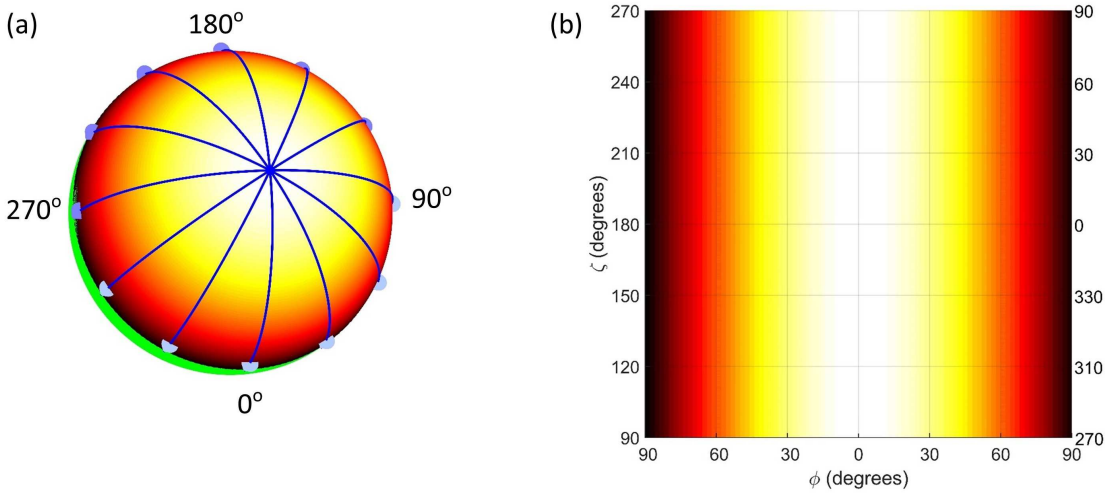

Fig. S5 (a) Full catalytic cap covering one hemisphere of the sphere and depicting the azimuthal angle (ζ) positions. The colour of the cap indicates the thickness of the evaporated metal (see colour bar, tables 1 to 3). The propulsion direction lines are shown in blue (see main text for an explanation). (b) A 2D "unwrapped" representation of the catalytic cap thickness as a function of azimuthal angle (ζ) and elevation angle (ϕ).

In Figure S5 (a) we have plotted a 3D representation of a full catalytic cap such as would be found for widely separated particles (see main article). The colour of the cap indicates the thickness (see colour bar, tables 1 to 3). Shown in blue

are the motion lines, which in the case of the full cap are balanced in all directions (see main article). Figure S5 (b) is an "unwrapped" representation of the 3D catalytic cap. In tables 1 to 3 we have plotted both the 3D and 2D representations of the catalytic cap for $\alpha = 0^o, 15^o$ and 30^o and $10^o \leq \theta \leq 80^o$.

Table 1 Results of modelling the evaporation of a metal onto a hexagonal arrangement of touching spheres, where the angle of rotation of the spheres is $\alpha = 0^o$ and the range of grazing angles of the metal vapour is $10^o \leq \theta \leq 80^o$. The dashed line indicates the position of the equatorial boundary of the full catalytic cap. Colour bar indicates the catalytic cap thickness in nm.

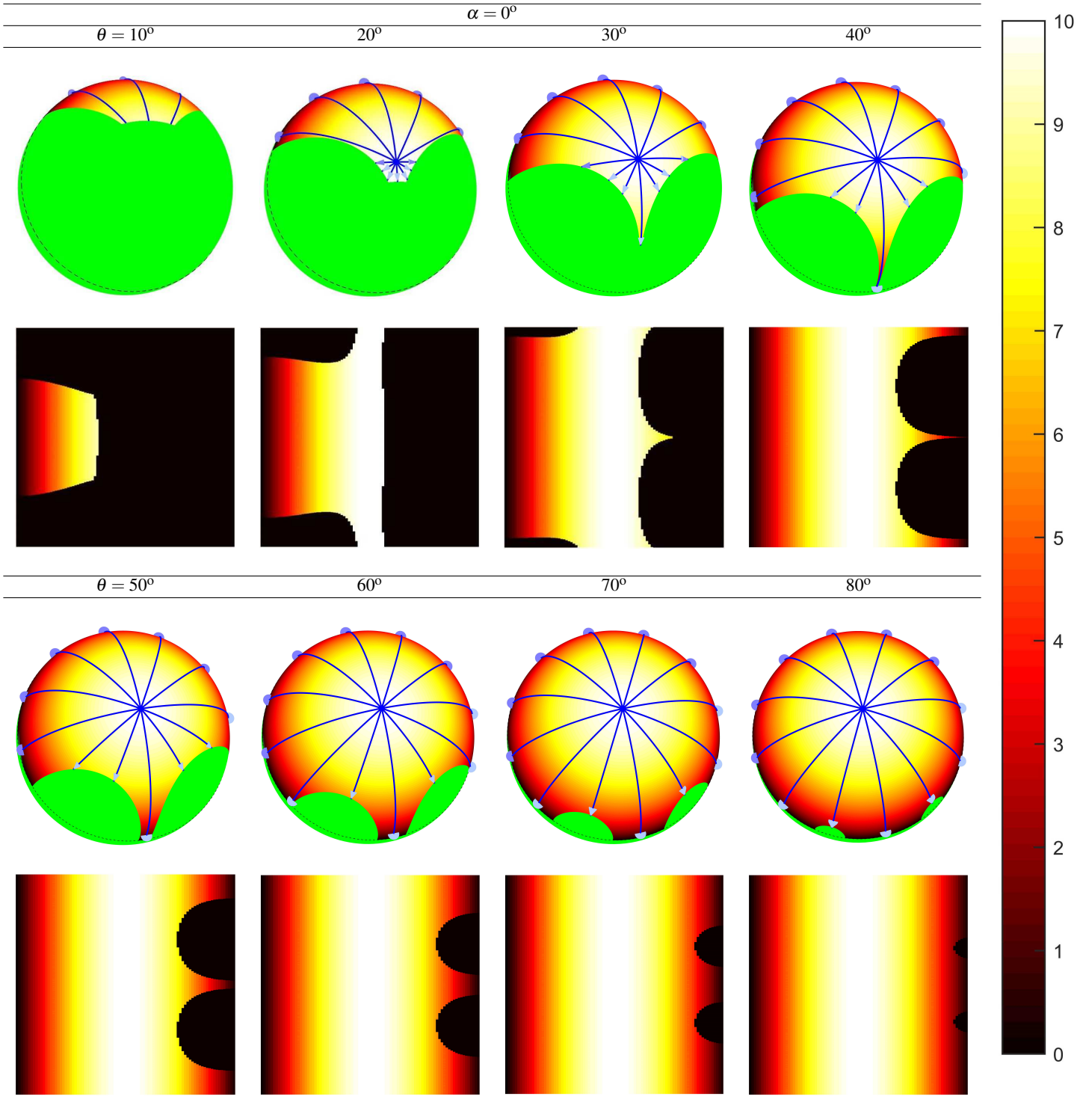

Table 2 Results of modelling the evaporation of a metal onto a hexagonal arrangement of touching spheres, where the angle of rotation of the spheres is $\alpha = 15^{o}$ and the range of grazing angles of the metal vapour is $10^{o} \leq \theta \leq 80^{o}$. The dashed line indicates the position of the equatorial boundary of the full catalytic cap. Colour bar indicates the catalytic cap thickness in nm.

$\alpha = 15^{o}$			
$\theta = 10^{o}$	20^{o}	30^{o}	40^{o}
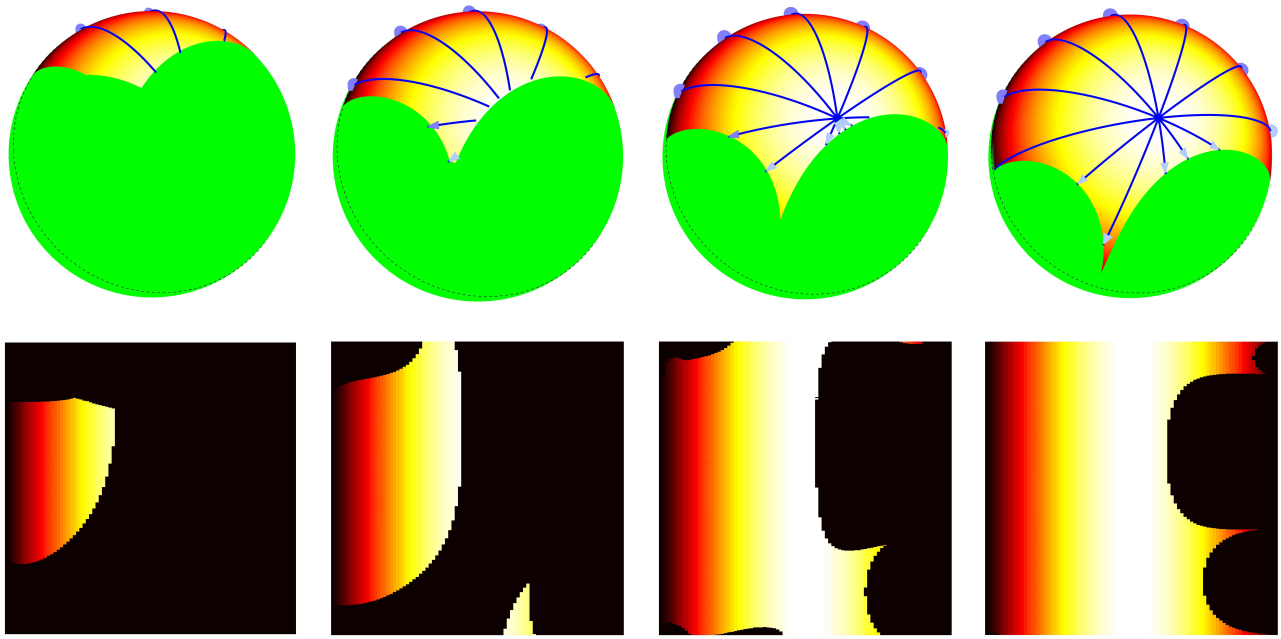			
$\theta = 50^{o}$	60^{o}	70^{o}	80^{o}
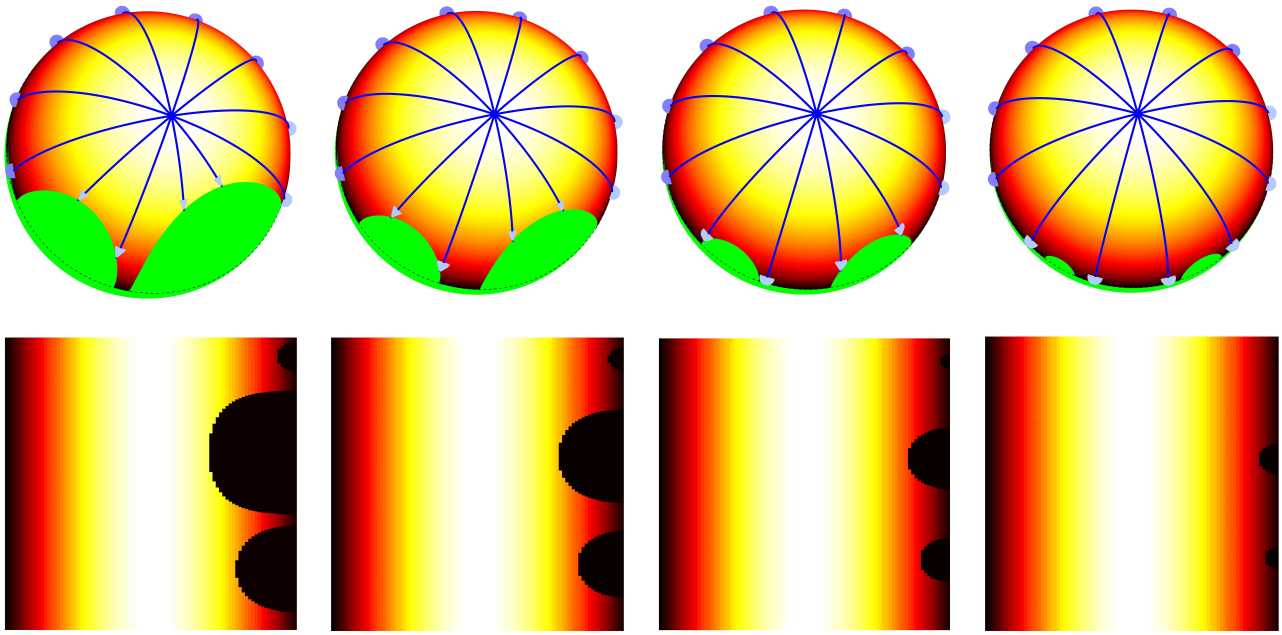			

Table 3 Results of modelling the evaporation of a metal onto a hexagonal arrangement of touching spheres, where the angle of rotation of the spheres is $\alpha = 30^{o}$ and the range of grazing angles of the metal vapour is $10^{o} \leq \theta \leq 80^{o}$. The dashed line indicates the position of the equatorial boundary of the full catalytic cap. Colour bar indicates the catalytic cap thickness in nm.

$\alpha = 30^{o}$			
$\theta = 10^{o}$	20^{o}	30^{o}	40^{o}
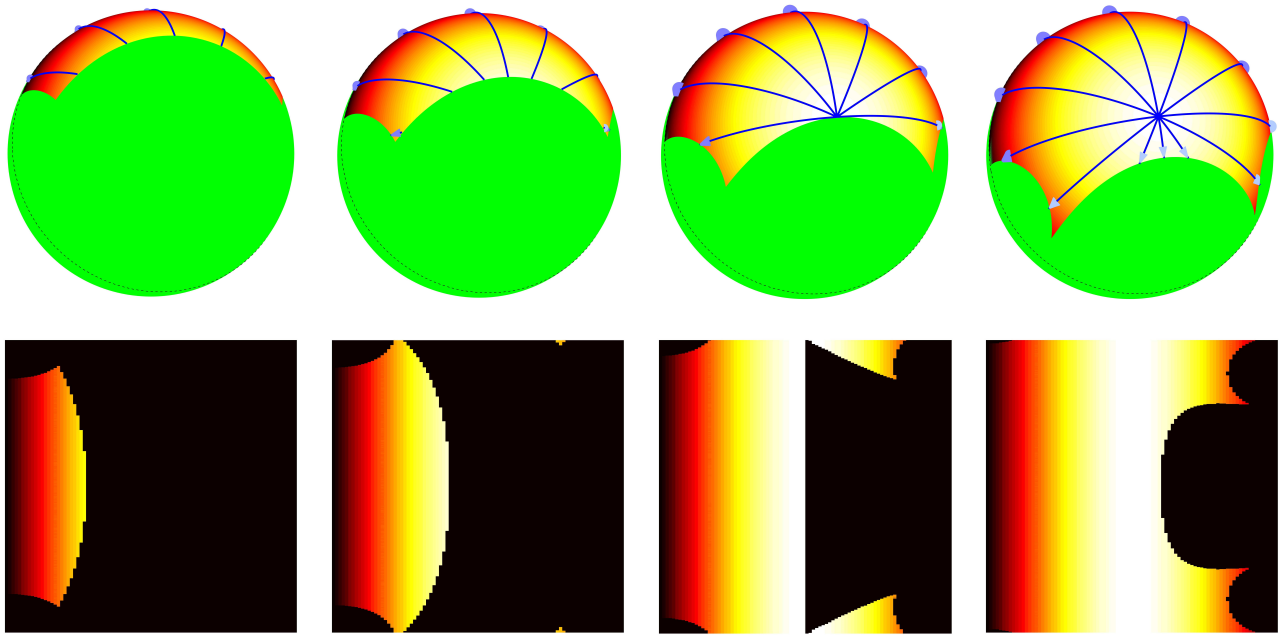			
$\theta = 50^{o}$	60^{o}	70^{o}	80^{o}
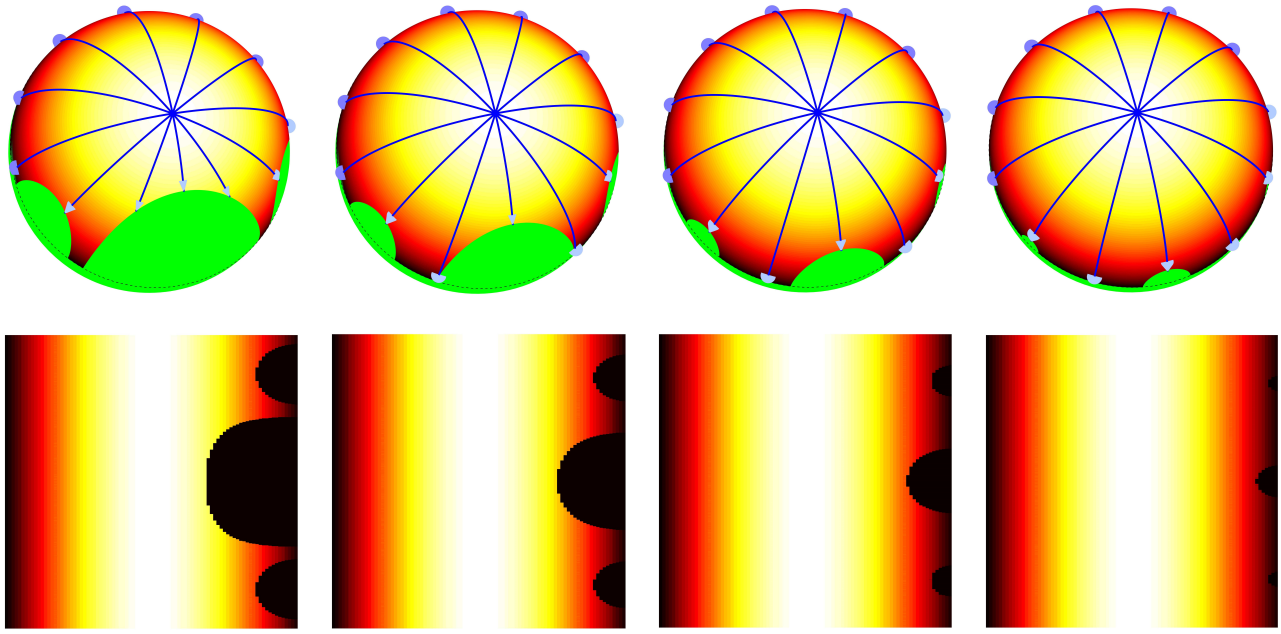			

References

1 A. B. Pawar and I. Kretzschmar, *Langmuir*, 2008, **24**, 355–358.

2 A. I. Campbell and S. J. Ebbens, *Langmuir*, 2013, **29**, 14066–14073.